



Green synthesis of LiZnVO₄ nanoparticles and its multiple applications towards electrochemical sensor, supercapacitor, humidity sensing, photoluminescence and antioxidant activities

T. L. Soundarya¹, Udayabhanu^{2,3}, Y. T. Ravikiran⁴, B. Nirmala^{1,*}, and G. Nagaraju^{2,*}

¹Department of Studies and Research in Chemistry, University College of Science, Tumkur University, Tumakuru, Karnataka 572 103, India

²Energy Materials Research Laboratory, Department of Chemistry, Siddaganga Institute of Technology, Tumakuru, Karnataka 572 103, India

³Center for Research and Innovations, BGSIT, Adichunchanagiri University, B. G. Nagara, Mandya District, Javarana Hally, Karnataka 571449, India

⁴Department of PG Studies in Physics, Government Science College, Chitradurga, Karnataka 577501, India

Received: 5 January 2022

Accepted: 10 March 2022

Published online:
24 March 2022

© The Author(s), under exclusive licence to Springer Science+Business Media, LLC, part of Springer Nature 2022

ABSTRACT

LiZnVO₄ nanoparticles (NPs) were synthesized by a simple combustion method using *Hibiscus Rosa Sinensis* leaves as a novel fuel and the prepared NPs were characterized using XRD, FT-IR, morphological analysis by SEM and TEM studies, elemental analysis by EDAX and ICP-MS. XRD data of the synthesized NPs were well-matched with the JCPDS number 038–1332 and it confirms the distorted phenacite structure of LiZnVO₄. FT-IR strengthens the bonding of M-M and M–O in LiZnVO₄. Optical characteristics of LiZnVO₄ NPs were studied by photoluminescence (PL) spectroscopy. Vanadate group of the prepared NPs originates a green emission. Examination of latent finger prints (LFP's) showed a crystal clear patterns under near UV region (365 nm) as they are the prominent techniques in crime investigations. LiZnVO₄ NPs exhibit a strong antioxidant property and act as a good sensor to detect sodium nitrite analyte at extremely low concentrations with limit of detection of 27.5 nM. Three-electrode system supercapacitor device has been fabricated and examined the performances. Specific capacitance of LiZnVO₄ NPs based supercapacitor was found to be 88.7 F/g at a current density of 0.1 mA. Power density (P_d) and energy density (E_d) were found to be 0.51 W/g and 12.3 Wh/Kg, respectively. This device exhibits a stable CV curves up to the scan rate of 10 V/s. Furthermore, LiZnVO₄ NPs acts as an excellent material towards the humidity sensing with a sensitivity factor, sensitivity and limit of detection of 28.0, 0.3 MΩ/%RH

Address correspondence to E-mail: nirmala2528@gmail.com; nagarajugn@gmail.com

and 5%RH, respectively. All the above studies show the diverse potentiality of LiZnVO₄ NPs.

1 Introduction

At present, nanotechnology is one of the leading fields in analytical technique of chemical science. Metal oxide nanoparticles found diverse applications for the fabrication of analytical tools. In that direction, materials scientists were observed that mixed metal oxides shows enhanced performances in comparison with its metal oxides. Recent literature survey and also of research interest allows to select LiZnVO₄ as one of the prominent materials to explore diverse applications including biological, chemical and medicinal fields. But in chemical, development of antioxidants is essential in annihilating several diseases as they slow down the activity of hazardous reactive groups such as reactive oxygen species (ROS) which includes hydroxyl radicals ($\cdot\text{OH}$), superoxide and peroxide radicals (O_2^- and O_2^{2-}), singlet oxygen ($^1\text{O}_2$) and peroxy radicals [1]. Hence, a substantial research is focused on the conversion of nanomaterials into useful antioxidants.

Electrochemical sensing can be used as the technique for detecting and measuring the analyte at different concentration level. Depending on the unique features of nanomaterials, they have been extensively used in many applications. Also, they play characteristic roles in several electrochemical sensing methods such as promotion of electron transfer, catalysis, labeling of biomolecules, as a reactant and in the immobilization process of several biomolecules [2]. Sodium nitrite is weakly toxic. In animal tissues, nitric oxide, a neurotransmitter, undergoes metabolism to produce nitrite. Sodium nitrite leads methemoglobinemia in omnivorous animal like swine and lowers the quantity of oxygen liberated from haemoglobin, in this way the animal lacks its strength and then die [3]. It has the ability to bring about tumors and grow up the malignancy. Therefore, quantification of nitrite at low concentration level is essential. Various methods are available to probe this analyte. However, electrochemical detection is more achievable when contrasted to other methods [4]. Nanomaterials modified sensors are effective in detecting sodium nitrite at very low

concentration levels by employing electrochemical voltammetric technique.

Energy is truly necessary these days as energy issues are a big challenge in the twenty-first century. Supercapacitors are considered as excellent devices for the storage of energy due to their high power density, high load currents, fast charging, long cycling life, operational safety, etc., hence, the development of them is very essential. Humidity sensors found most useful applications such as in Pharmaceuticals, agriculture, food processing, etc., which estimates the presence of moisture content and also the material's resistance there by its sensitivity can be determined. The higher the humidity sensing activity of the material, the higher will be the capacitance of it. In this report, efforts have been made in developing the LiZnVO₄ based supercapacitors and in determining the specific capacitance by a simple procedure using cyclic voltammetry and galvanostatic charge and discharge technique.

LiZnVO₄, a trimetallic oxide, a vanadate based material, found applications in energy storage devices such as Li-ion battery [5–7] and optical properties [8] due to its arrangement of atoms in a crystal lattice and advanced redox chemistry of vanadate group. Zeng et al. have synthesized it from hydrothermal method [5] for Li-battery applications. Yunyan et al. have synthesized it from solid state reaction at high temperature of 750 °C [6] for electrochemical measurements. In this report, we have emphasized the synthesis by simple, non chemical, green fuel assisted, solution combustion route using Hibiscus rosa sinensis leaves as fuel. This method is exceptionally easy to produce the compound in mass for huge scope modern applications as other methods demand tedious procedures, time consuming and thorough experimental conditions such as high sintering and annealing temperatures and the possibilities of obtaining impurities are high in solid state synthesis. We are the first to report the antioxidant activity, Latent fingerprint development for crime investigations using a technique of plain LiZnVO₄ NPs based powder dusting technology, supercapacitor behavior and sensing activity of LiZnVO₄ NPs towards the

detection of nitrite at very low concentration and Humidity sensing of pure LiZnVO₄ NPs.

2 Experimental details

2.1 Preparation of LiZnVO₄ NPs

For the synthesis of LiZnVO₄ NPs by solution combustion route, precursors such as lithium nitrate, zinc nitrate and ammonium metavanadate are required (Merck India Ltd). Finely powdered hibiscus leaves were used as a fuel. Stoichiometric amount of the above precursors in 1:1:1 ratio along with the finely powdered hibiscus leaves of 600 mg were taken in the silica crucible having 3 mL of distilled water. The contents are stirred magnetically and introduced into the preheated, 500 °C temperature asserted muffle furnace. Combustion process was concluded in 5 min with the formation of yellowish white LiZnVO₄ NPs as a product.

2.2 Characterization

Crystal structure of the LiZnVO₄ NPs were analyzed by recording the XRD data of the sample using Rigaku-Smart Lab X-ray diffractometer with CuK_α (1.541 Å) radiation. FT-IR spectrum of the prepared sample was obtained with the aid of Bruker Alpha-p spectrometer from KBr pellet method. The surface morphology was analyzed using (Hitachi – 3000) Scanning electron microscope. TEM images were collected using FEI tecnai model. Elemental and trace elemental analysis were made by using EDAX and ICP-MS. Photoluminescence of LiZnVO₄ NPs was investigated by Cary eclipse fluorescence spectrophotometer (Agilent technologies). Developed LFP's on different surfaces were visualized through UV cabinet at 365 nm and the corresponding pictures were captured by Samsung Galaxy J7 rear camera with 13-mega pixels.

2.3 Antioxidant activity

Antioxidant activity of the prepared LiZnVO₄ NPs was studied by following the modified process of Brand-Williams [9] using 2,2-diphenyl-1-picrylhydrazyl (DPPH) assay. DPPH is a stable free radical, which is violet in color corresponding to its oxidized form. It exhibits a broad peak due to the maximum

absorption in the visible region (520 nm). As soon as an antioxidant entity gives an electron to the DPPH radical and its action was hindered. Consequently, adjustments in absorbance take place at the same wavelength. 19.7 mg of DPPH was liquefied in 50 mL methanol to acquire 0.14 mM concentration of DPPH. 50% methanol was prepared by diluting methanol with de-ionized water (1:1). Different concentrations of the test sample, such as, 20, 40, 60 and 80 µg were set up by blending relative volumes of sonicated LiZnVO₄. To this, 50% methanol was added such that it should make 1 mL when 140 µL of DPPH solution was added. The blend was incubated at 35 °C for about 30 min. A blank solution was prepared without adding the test sample, which is considered to be a control sample. Using a spectrophotometer, the absorbance of the samples was recorded at 520 nm, with reference to the blank solution. The difference between the absorbance of the blank solution and the test sample gives the actual absorbance, which is useful in estimating the percentage inhibition value of an antioxidant. By plotting the percentage inhibition against the concentration of the NPs, Inhibition concentration-50 (IC₅₀) can be determined.

2.4 Electrode modification and their electrochemical examination

2.4.1 Experimental

Complete electrochemical analysis was performed using Inc (Chi6111e) CH Instruments and an electrochemical cell of capacity 10 mL provided with three-electrode system, in which working electrode (glassy carbon electrode), auxiliary electrode (a platinum wire) and reference electrode (Ag/AgCl) were incorporated. pH of the solution was examined by employing a pH meter. 1 M NaOH aqueous solution and the potential range from – 1.2 to 1.2 V were set to obtain the CV curves. Specific capacitance (C_s) and the Energy density (E_d) of the prepared electrodes were calculated from the CV data using the Eqs. (1) and (2) [10]

$$C_s = \frac{\int IdV}{2m\Delta V_v} \quad (1)$$

$$E_d = \frac{C_s V^2}{2 * 3600} \quad (2)$$

where IdV represents the area of the CV, m is the mass of the active material deposited on the

electrode, ΔV is the potential window (2.4 V) and v is the selected scan rate (in mVs^{-1}).

2.4.2 Surface modification

Before modification, the glassy carbon electrode (GCE) was rinsed with DI water and polished manually with various grades of alumina particles to get a mirror finish. Then it was subjected to sonication with deionized water and ethanol for about 2 min. The dispersed solution of the LiZnVO_4 NPs was made by sonicating the solution of 5 mg of it in 1 mL of DI water. Then the corresponding solution was coated on the surface of the GCE by drop casting method and kept aside to air dry for 4 h.

3 Results and discussion

3.1 XRD studies

Premier characterization of LiZnVO_4 NPs was done using XRD studies as outlined in Fig. 1. The peaks of diffraction patterns are indexed to the rhombohedral crystal system with distorted phenacite structure, as the data obtained are in accordance with the JCPDS card number 038–1332. From the Debye–Scherrer Eq. (3), the average crystallite size of LiZnVO_4 NPs was estimated to be 67 nm.

$$D = \frac{K\lambda}{\beta \cos \theta} \quad (3)$$

where, D is the average grain size or crystallite size, λ signifies the wavelength of the X-ray, K is the

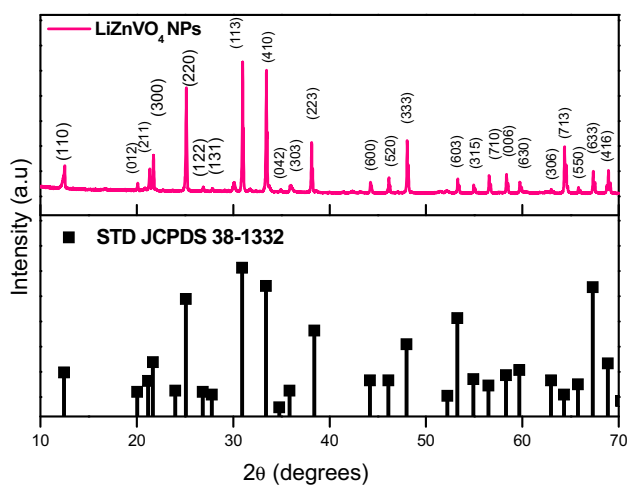


Fig. 1 XRD pattern of LiZnVO_4 NPs

crystallite shape factor (0.94), β is the full width at half maximum and θ is the Bragg's diffracting angle [11].

3.2 FT-IR studies

Synthesized LiZnVO_4 NPs were subjected to FT-IR analysis and the spectrum was recorded between 350 and 4000 cm^{-1} (Fig. 2). Different functional groups and the existence of metal–oxygen bonds in the sample were investigated from the FT-IR analysis. A huge vibration band ranging from 400 to 700 cm^{-1} is referred to the stretching of Zn–O bond [12]. The band at 480 cm^{-1} represents the vibrational stretching frequency of Li– VO_4 group [13]. Peak at 813 cm^{-1} , corresponding to V–O–V vibration of vanadate group [14]. Peaks at 1637 and 2920 cm^{-1} corresponds to C = C and C–H stretching, respectively. A peak corresponding to 3416 cm^{-1} specifies the O–H stretching and a less intense peak at 1637 cm^{-1} demonstrates the bending vibrations of O–H bonds, indicating the presence of moisture in the sample [15].

3.3 SEM studies

Figure 3. depicts the SEM image and EDAX of LiZnVO_4 NPs. SEM image distinctly exemplifies the cluster of particles formed from the agglomeration of NPs. They are more or less spherical in shape. The composition of LiZnVO_4 includes Zn, V and O as specified by EDAX.

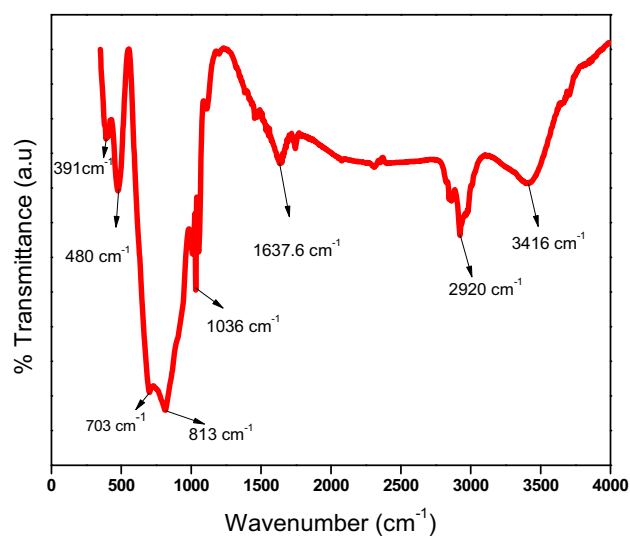


Fig. 2 FT-IR spectrum of LiZnVO_4 NPs

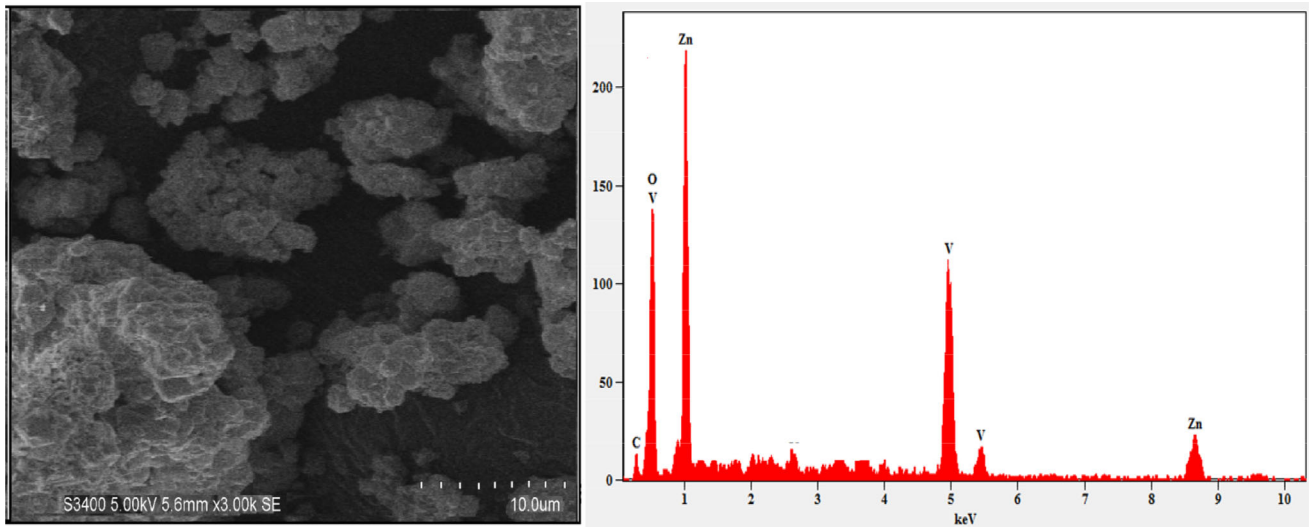


Fig. 3 SEM image and EDAX of LiZnVO_4 NPs

3.4 TEM studies

Figure 4. shows the (a–c) TEM images, (d) HR-TEM and (e) SAED pattern of LiZnVO_4 NPs. The sharp

edge structure of the phenacite LiZnVO_4 crystal is evident in the TEM images. The plane obtained from the d-spacing value of the HR-TEM image is well-matched with the (110) plane of the XRD pattern.

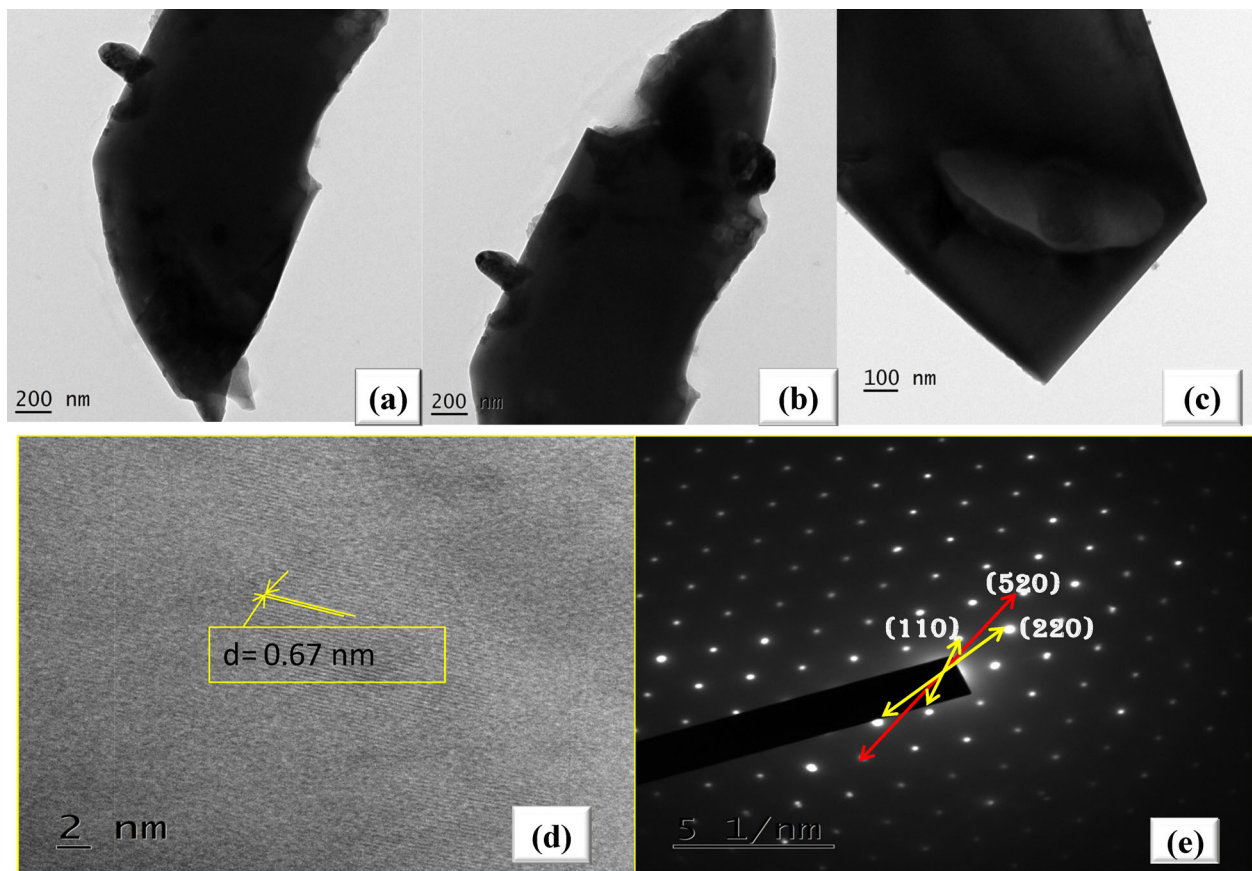


Fig. 4 a–c TEM images, d HR-TEM and e SAED pattern of LiZnVO_4 NPs

Bright spots in the SAED pattern indicate the high crystalline nature of the material and the presence of XRD planes (110), (220), and (520) is confirmed by the SEAD pattern.

3.5 ICP-MS studies

To detect the metals present in the liquid sample of LiZnVO_4 NPs, a chemical characterization was carried out with the aid of inductive coupled plasma mass spectrometry studies (ICP-MS). Liquid sample was prepared at extremely low concentrations by digesting solid LiZnVO_4 NPs in con. HNO_3 and water for 20 min at 80 °C with dilution factor of 1000. Blank solution of '0' ppb and concentration of 100 ppb solution was prepared and used as standard solution. Certified concentrations of Li, Zn and V with concentration and uncertainty of 100.0 ± 0.5 mg/L were used as reference. The

following table and Fig. 5. Illustrate the concentration of elements present in the liquid sample.

4 Photoluminescence studies

Semiconductor's charge separation and the electronic structure of the material can be probed by PL studies. The excitation and emission spectrum of LiZnVO_4 NPs show a band at 337 nm and 533 nm, respectively, as depicted in Fig. 6a and b. A peak was observed at 324 nm in the excitation spectrum. CIE (Commission International D'Eclairage) diagram was plotted (Fig. 6c), the color of light emission was found to be light green, and it is indicated by an asterisk mark on the CIE diagram. The chromaticity coordinates were estimated to be $X = 0.33101$ and $Y = 0.45136$ which is suited for green emission and these factors proves that the prepared LiZnVO_4 NPs

Element	Mass	Concentration from ICP-MS report	Concentration of elements present in sample solution
Li	7	73792121.4 ppb	7.3792×10^{10} ppb
Zn	66	196066292.8 ppb	19.6066×10^{10} ppb
V	51	1314280.8 ppb	13.14280×10^9 ppb

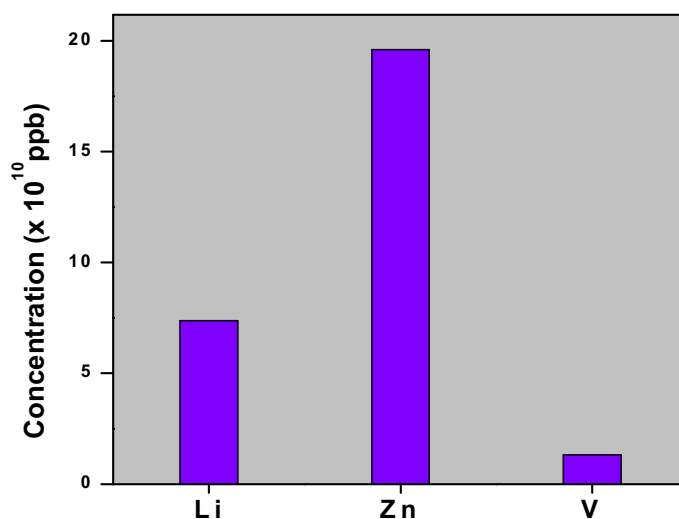


Fig. 5 ICP-MS results showing concentration of elements in sample

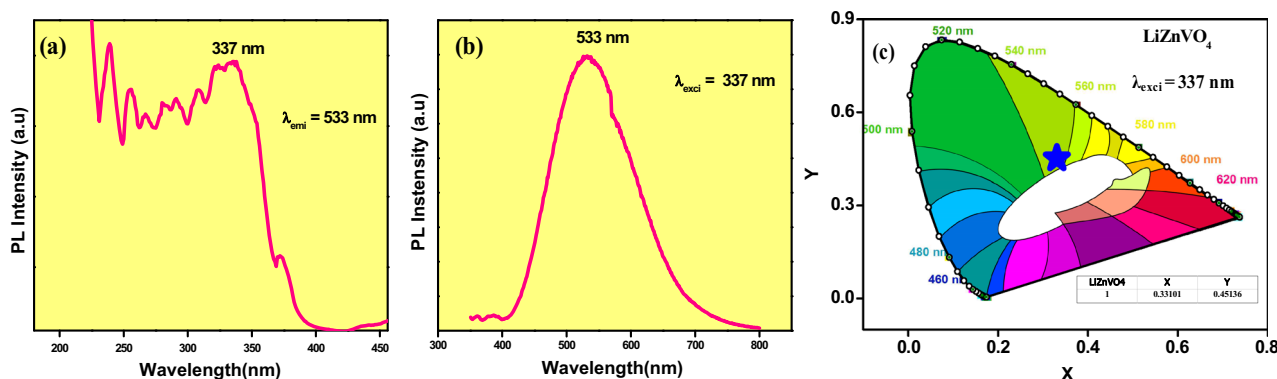


Fig. 6 a Excitation b Emission spectrum and c CIE diagram of LiZnVO₄ NPs

can be successfully used for the Light Emitting Diode applications (LEDs) [16–18].

4.1 Latent fingerprint applications

We all know that human fingerprints are extremely unique. It differentiates from person to person and hence this feature is most importantly used in forensic applications. But LFP's are not visible to the naked eye and require additional processing techniques. LFP's may be developed from several methods such as powder dusting, ninhydrin dipping, iodine fuming and silver nitrate soaking [19, 20]. All these methods have their own disadvantages like low resolution, cost effect and background noise. In the present study, we have utilized the method of powder dusting which is easier and quick method. Scheme 1 explains the procedure for the development of LFP's. LFP's were created on rigid surfaces such as a beaker, a CD, and a knife. The represented fingerprints contain eye, loops, whorls, and arches. Additionally, the clear ridge structures of the Fingerprints can be clearly detected without any obstruction. As a result, the prepared LiZnVO₄ NPs can be regarded as the best material for LFP's applications (Fig. 7).

5 Antioxidant studies

DPPH is generally used to assess the capacity of compounds to function as free radical scavengers or hydrogen radical donors and to estimate the antioxidant activity [21]. The principle behind the molecule showing antioxidant property can be depicted as; in the presence of antioxidants, DPPH diverges from violet to yellow color analogous to its reduced form

[22]. This is because of the oxidation of prepared NPs and reduction of the DPPH radical by the movement of either electrons or hydrogen radicals from the sample, neutralize the DPPH and then DPPH turns yellow color, as depicted in the scheme 2.

By observing the concentration of DPPH and furthermore, by estimating the decrement in the DPPH absorbance around 520 nm, antioxidant activity of the sample was assessed [23].

The percentage (%) of inhibition of the DPPH can be determined using Eq. (4)

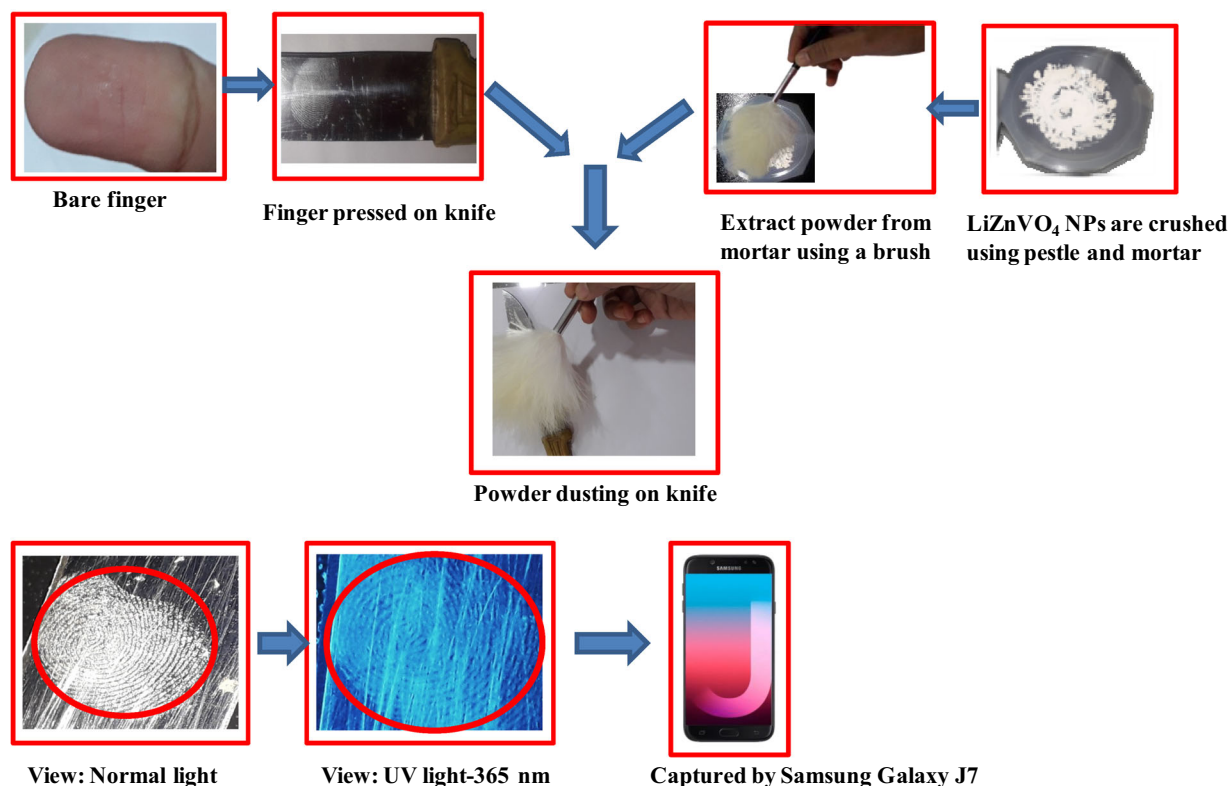
$$\% \text{ of Inhibition} = \frac{A_i - A_o}{A_i} * 100 \quad (4)$$

where A_i is the absorbance of the control and A_o is the absorbance of the sample solution [24].

From the Fig. 8, IC₅₀ value was found to be 37.32 µg/mL which is very low and accordingly the synthesized LiZnVO₄ NPs can be utilized as an acceptable antioxidant agent [25].

6 Electrochemical functioning of LiZnVO₄ NPs: sensing of sodium nitrite

In order to examine the electrochemical performance of the prepared LiZnVO₄ NPs, cyclic voltammetric technique has been adopted using sodium nitrite as a model system. CV's of nitrite at bare GCE, at GCE with 5 mM concentration of nitrite and LiZnVO₄ coated GCE with 5 mM of nitrite solution were recorded using phosphate buffer of pH 12.0 with a scan rate of 50 mV/s, shown in Fig. 9. A kind of simple line was observed with bare GCE, representing an action of electron transfer has not yet started



Scheme 1 Development of Latent fingerprint using LiZnVO_4 NPs

because of the absence of the analyte (Curve c in Fig. 9). Without analyte, LiZnVO_4 modified glassy carbon electrode ($\text{LiZnVO}_4/\text{GCE}$) didn't show any voltammetric signature in the given potential window, signifying that $\text{LiZnVO}_4/\text{GCE}$ can be used as a sensor towards the nitrite detection. Curve (b) and (a) of Fig. 9 represent the characteristic oxidation peaks corresponding to the bare GCE and $\text{LiZnVO}_4/\text{GCE}$ in the presence of nitrite, respectively. Increased peak current with low potential was observed for $\text{LiZnVO}_4/\text{GCE}$ when compared to bare GCE indicating the electro catalytic effect of modified surfaces.

Furthermore, the oxidation peak of nitrite for the $\text{LiZnVO}_4/\text{GCE}$ was observed at 1.16 V. Peak current was found to be nearly 2 times greater than that of bare GCE, proposing the electrocatalytic movement of LiZnVO_4 towards the oxidation of nitrite analyte, which can be accounted its unusual basic features and spectacular electrochemical properties [26].

6.1 Effect of pH

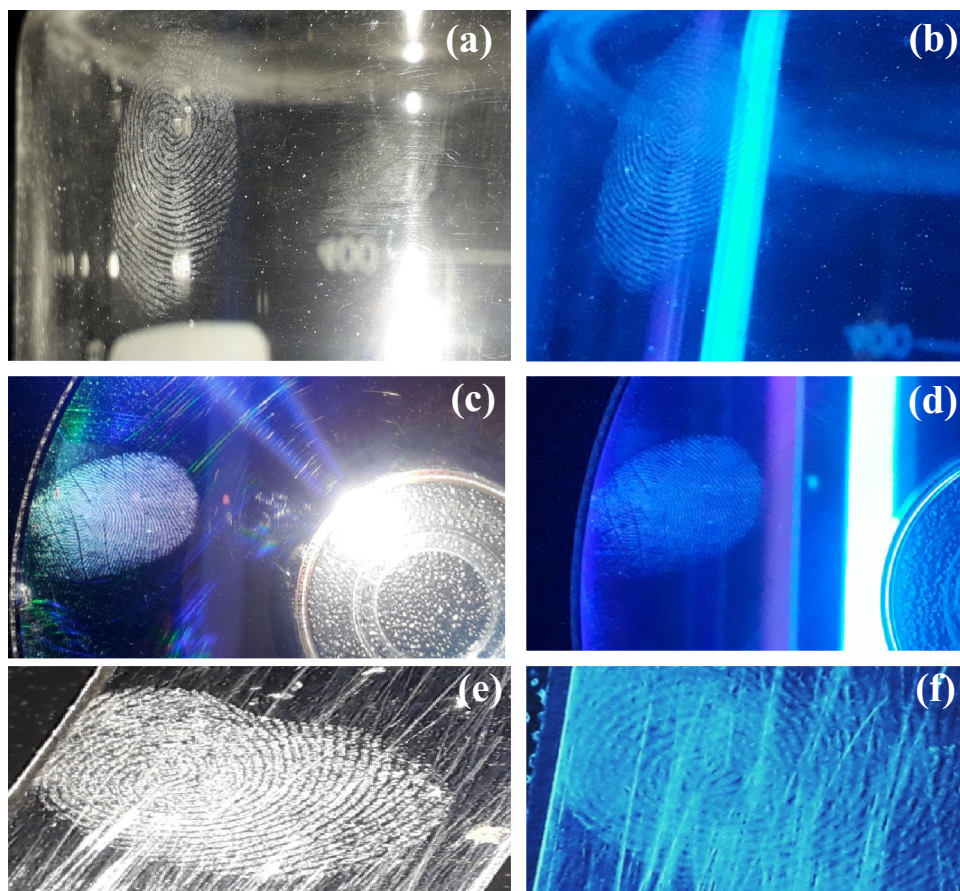
The impact of pH on peak current was examined over the pH range from 2 to 12.0 using phosphate

buffer solutions, as shown in Fig. 10. Nitrite response was assessed using $\text{LiZnVO}_4/\text{GCE}$ in presence of 2 mL of 5 mM of nitrite solution. With extending pH, the current raises and extended to the utmost value at $\text{pH} = 12$. In this mode, the buffer solution of $\text{pH} = 12$ was chosen as the working medium for further studies. This shows that, strong basic condition was important to get a better current response due to decreased participation of protons in the electrode reaction. Similarly, it showed that the peak potential is also dependent on the pH.

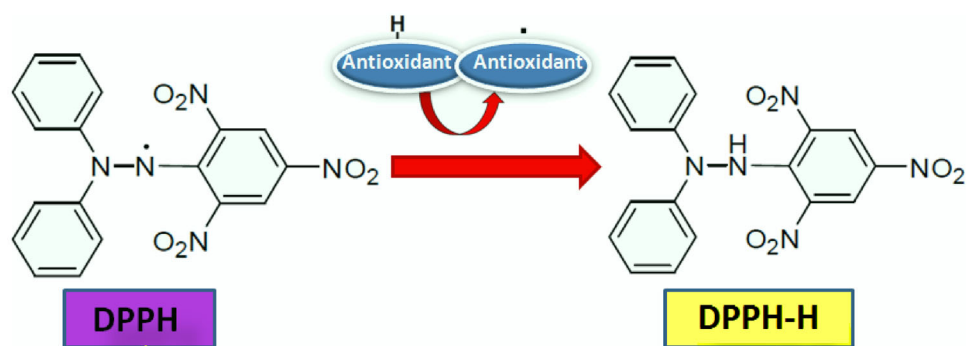
6.2 Variation of scan rate: effects on nitrite oxidation

To know the impact of scan rate on peak currents was examined by conducting the cyclic voltammetry of 2 mL of 5 mM nitrite at various scan rates starting from 50 mVs^{-1} to 150 mVs^{-1} using $\text{LiZnVO}_4/\text{GCE}$ in the presence of buffer pH 12, as depicted in Fig. 11. In order to determine whether the electrochemical reaction is diffusion controlled or adsorption controlled, a plot of log of current versus log of scan rates was drawn (Fig. 12). From this graph, it is confirmed

Fig. 7 Images of LFP's developed on **a, b** Beaker **c, d** CD and **e, f** Knife



Scheme 2 Reaction between free radicals and antioxidants



that the electrochemical reaction of nitrite is diffusion controlled [27] as its slope was found to be 0.4322 which is closer to 0.5 with the linear regression equation $\log(I) = 0.4322 \log(\text{scan rate}) - 3.94906$ having R^2 value of 0.98031 and the surface of modified GCE was not defiled by them.

6.3 Effect of concentration on electrochemical oxidation of nitrite

Electrochemical sensing of nitrite was further investigated by changing the concentration of nitrite from 0.5 μM to 5 μM by keeping the scan rate (50 mV/s) and pH buffer solution (pH = 12) as constant and is shown in the Fig. 13. Peak currents were extended moderately with the increment of nitrite concentration, as shown in Fig. 14. From this plot, a linear regression was obtained to be $I_p = 3.00 C + 1.757$

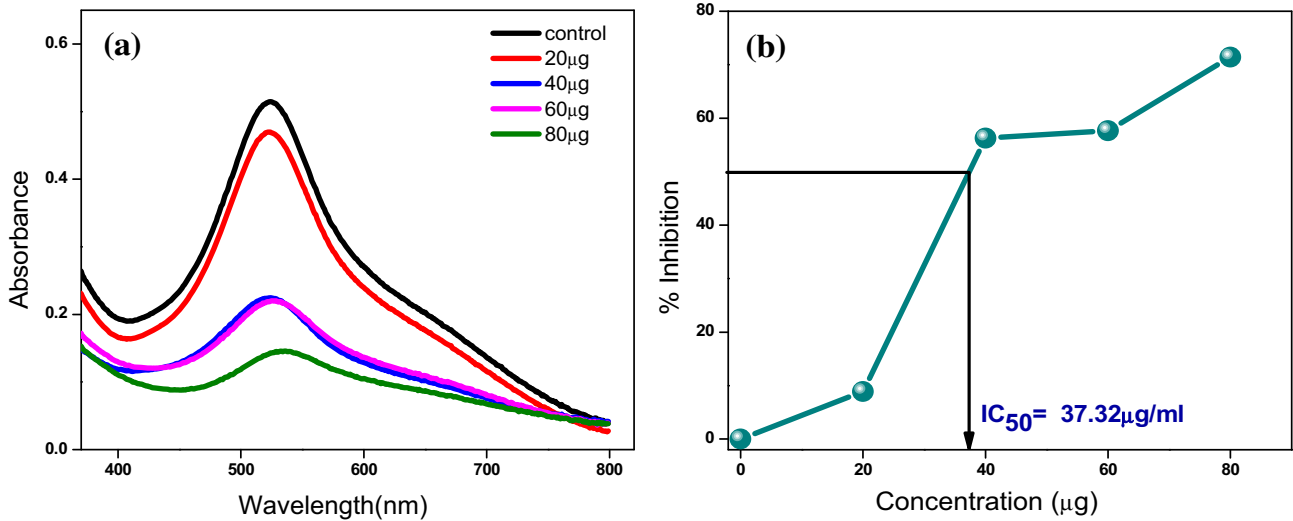


Fig. 8 a Antioxidant activity and b IC₅₀ value of LiZnVO₄ NPs

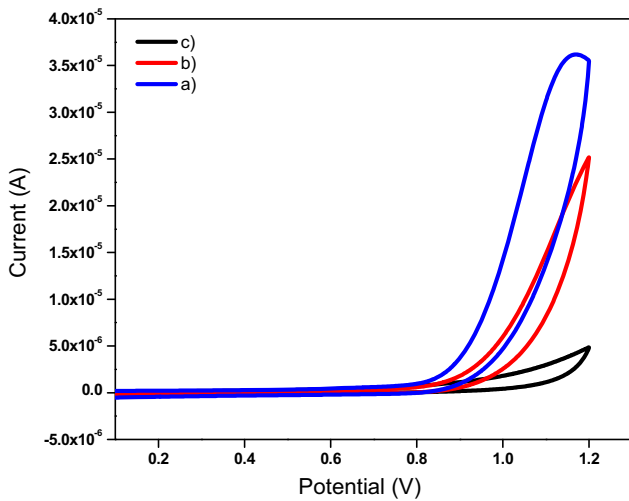


Fig. 9 CV profile of (c) GCE without nitrite, (b) GCE in the presence of 2 mL of 5 mM of nitrite and (a) LiZnVO₄/GCE in the presence of 2 mL of 5 mM of nitrite in a phosphate buffer solution of pH 12.0 with a scan rate, 50 mV/s

where I_p is in μA and C in μM , respectively. The limit of detection for nitrite detection was calculated to be 27.5 nM which is obtained from $3S_b/m$, where S_b is the standard deviation for the 5 independent cyclic voltammetric response recorded for the blank solution. As the detection limit is too low, LiZnVO₄ NPs based sensor can be used as a sensible candidate for the detection of nitrite.

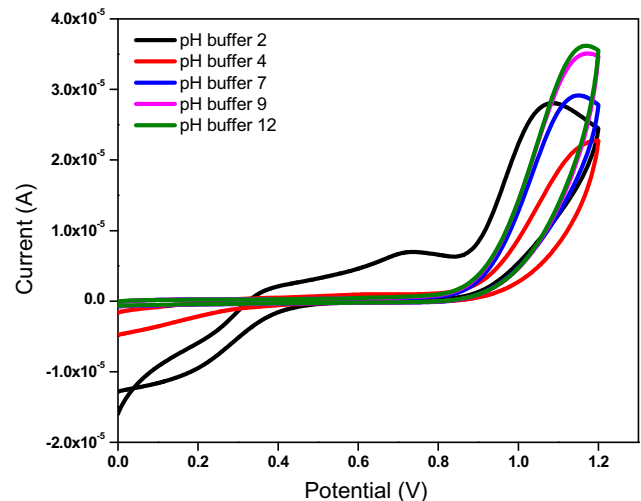


Fig. 10 Effect of pH buffer on peak currents of the nitrite at a scan rate of 50 mVs⁻¹

6.4 Stability analysis

Stability of LiZnVO₄/GCE towards the detection of nitrite was studied using 5 mM nitrite, KCl and pH 12 solution following the same procedure as described previously. The CV performance of LiZnVO₄/GCE has been studied persistently for seven consecutive days. A plot of current vs. time is shown in Fig. 15. and inset shows the percentage of current retention. Almost constant currents is observed upto the 7th day and the variation of current was very small. Peak currents at 1st day and 7th day were found to be 3.09×10^{-5} and 2.99×10^{-5} A, respectively. Current retention was found to be 97% at 7th

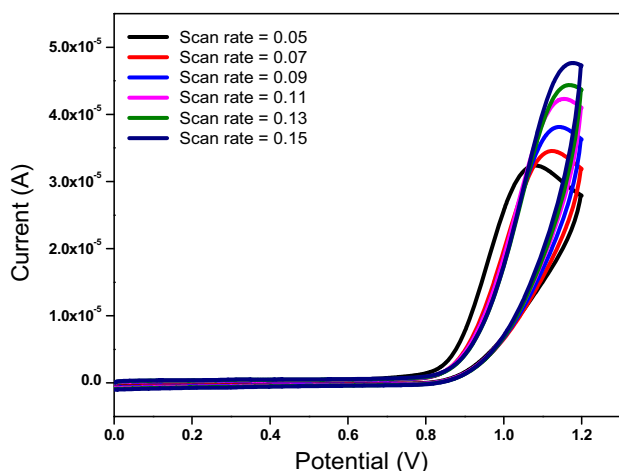


Fig. 11 Variation of peak current with the scan rates ranging from 50–150 mVs⁻¹ using CVs of LiZnVO₄/GCE in pH Buffer 12

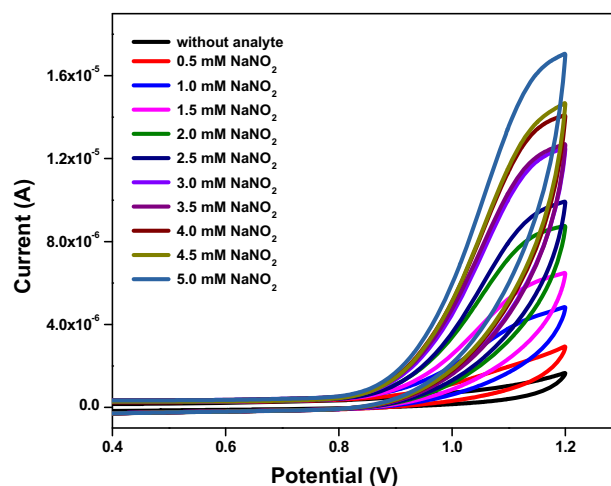


Fig. 13 CV's for nitrite at the LiZnVO₄/GCE in the presence of 2 mL of 5.0 mM nitrite in a buffer solution (pH = 12.0)

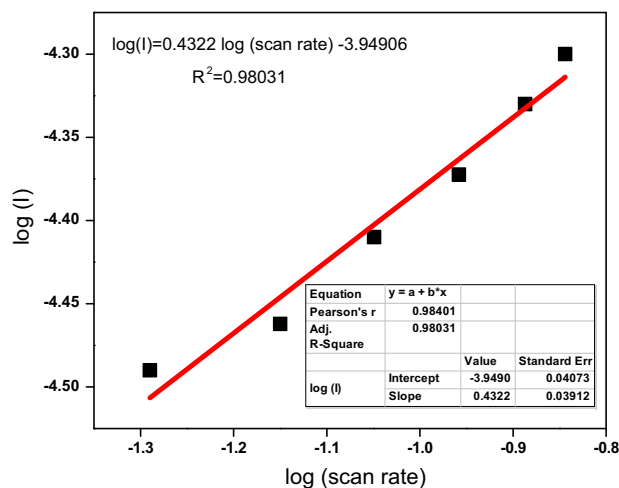


Fig. 12 Shows the linear relationship of the log of current versus log of scan rate

day. These results suggest that LiZnVO₄ NPs based sensors are more stable towards the detection of nitrite.

7 Electrochemical supercapacitive behavior of LiZnVO₄ NPs: Energy storage applications

The supercapacitive characterizations of the prepared materials have been studied using 3-electrode system subjected to various scan rates using cyclic voltammetric method. Figure 16a. shows the CV curves for the prepared LiZnVO₄ electrode with varied scan rates. Scan rates were varied from 20 mVs⁻¹ to 10,000

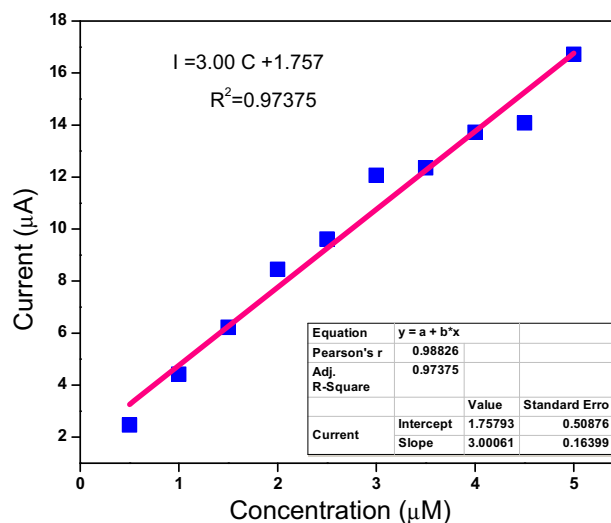


Fig. 14 Linear relationship of the current versus concentration of nitrite

mVs⁻¹. The system produced stabilized CV curves even at high scan rate of 10,000 mVs⁻¹ and this high scan rate is uncommon and rarely reported in the literature [28].

The most widely utilized scan rates are below 1 V/s. Here, it is started with a 20 mVs⁻¹ scan rate and a C_s was obtained to be 11.034 F/g corresponding to the discharge current (I) of 4.1 μA/g. Then the scan rate was increased to 50, 100, 200, 300, 400, 500 mVs⁻¹ and the C_s's were found to be 10.23, 8.41, 7.35, 6.65, 6.23 and 5.91, respectively. C_s was found to be 3.076 F/g at 10,000 mVs⁻¹. At 20 mVs⁻¹, the area of the CV curve was very small, as the scan rate increases; area

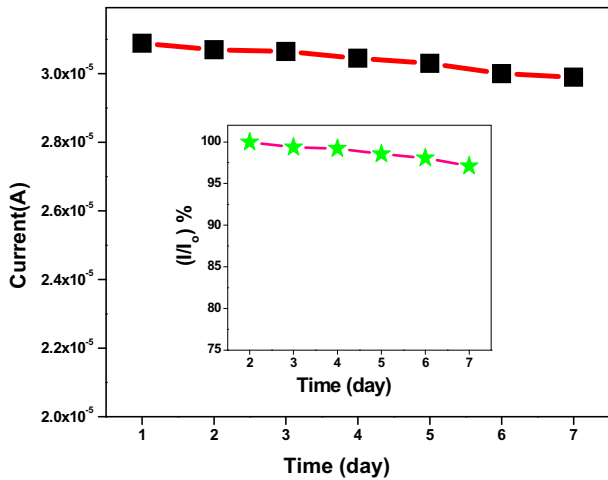


Fig. 15 Stability of LiZnVO₄/GCE over 7 days. (Inset plot is the % of current retention)

of the CV curves also increases, without changing in the curve shape.

As shown in Fig. 16c, discharge currents increased linearly with increasing scan rate. It was initially 4.1, 8.55 and 14.5 $\mu\text{A/g}$ for 20, 50 and 100 mVs^{-1} respectively. Later, it was raised to 208, 266, 311 and 532 $\mu\text{A/g}$ for 3000, 4000, 5000 and 10,000 mVs^{-1} , respectively. But C_s of the electrode decreases with increasing scan rate shown in Fig. 16d which is a familiar trend. At a very low scan rates, particles in the electrolyte have adequate time and the chance to enter the material through openings, however, they gather on the external surface of the electrode at higher scan rates.

Potential-electrochemical impedance analysis (PEIS) was performed using Biologic EC-Lab model.

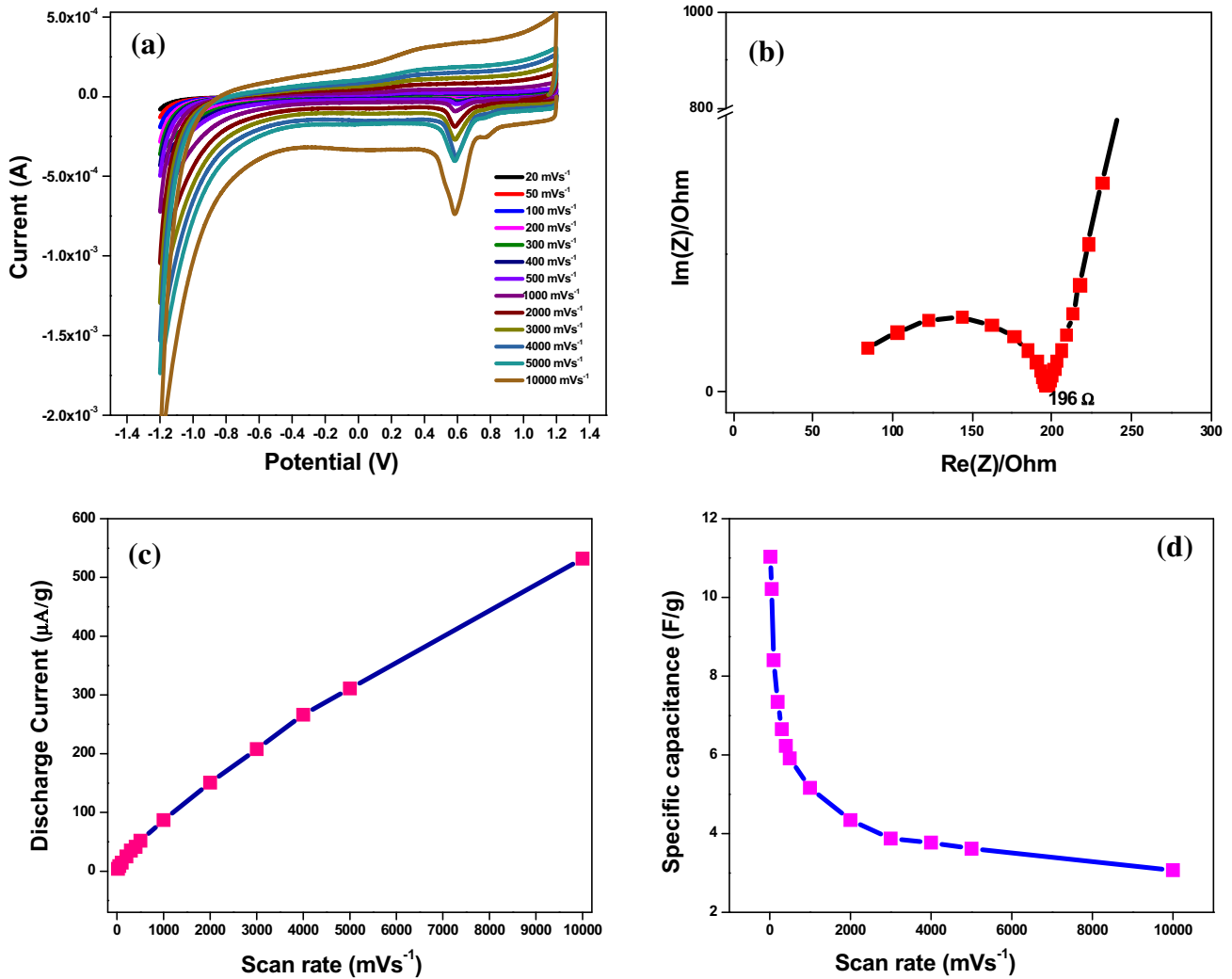


Fig. 16 a Cyclic voltammetric curves at the potential range of -1.2 to 1.2 V. b EIS of LiZnVO₄ NPs c Discharge currents and d Specific capacitance as a function of Scan rates

Charge transfer resistance (R_{CT}) was obtained from the diameter of the semicircle part of the spectrum and linear part of it reveals about the capacitance of the material (Fig. 16b). Z- fit analysis was performed to know the equivalent circuit for the obtained plot. R_{CT} was found to be 117 Ohm, which was obtained from the difference of final and initial resistance of the semicircle. The equivalent circuit was found to be $C_1/(R_1 + C_2/R_2 + M_3)$ as shown in Fig. 17d, where C_1 , C_2 are the capacitances, R_1 and R_2 are the resistances and M is the restricted diffusion.

Energy density of the LiZnVO_4 coated electrode was found to be 8.83 mWhkg^{-1} with a C_s of 11.034 F/g and C_s at an ultra high scan rate of, $10,000 \text{ mVs}^{-1}$ was found to be 3.1 F/g .

Electrochemical energy storage of LiZnVO_4 NPs-based supercapacitor can be furthermore analysed by subjecting it to galvanostatic charge–discharge (GCD) technique at different current densities. The resultant capacitive performance was observed from E-T curves with current densities of 0.1, 0.15, 0.2 and 0.24 mA, as shown in Fig. 17a.

The C_s 's are acquired from the GCDs using Eq. (5) were found to be 88.7, 85, 79, 76.3 and 60.8 F/g at current densities of 0.1, 0.15, 0.2 and 0.24 mA, respectively, as shown in Fig. 17c. This shows the decrease of C_s 's with increasing in current rate.

$$P_d = \frac{E_d * 3600}{\Delta t} \quad (5)$$

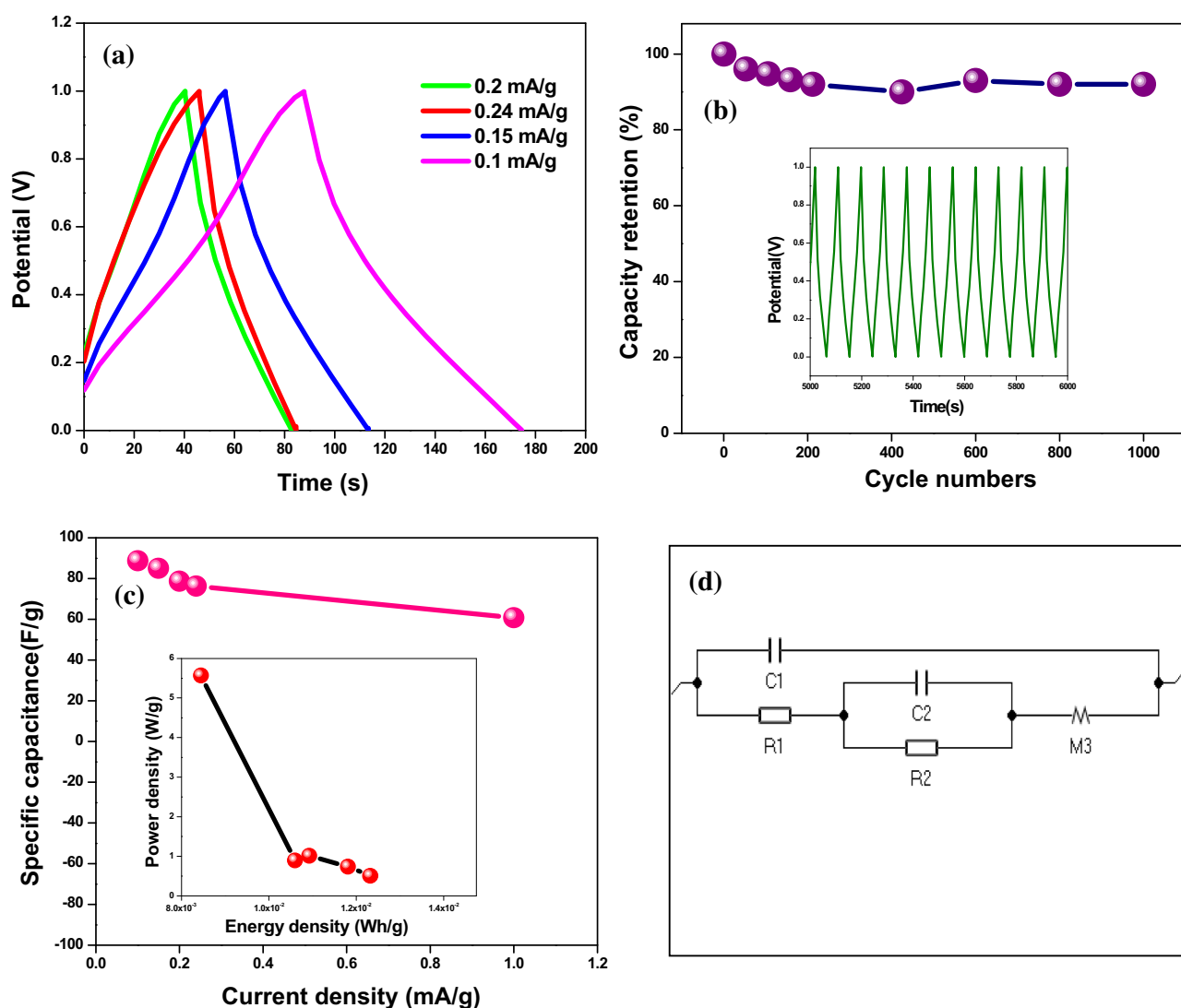


Fig. 17 a GCD curves at different current densities. b Cycling stability (inset) and capacity retention of LiZnVO_4 NPs-based supercapacitor. c Ragone plot (inset) and Rate capability of LiZnVO_4 NPs. d Equivalent circuit for the PEIS

where, E_d is the energy density and Δt is the discharge time.

Cycling stability of LiZnVO_4 NPs-based supercapacitor was examined at a current density of 0.24 mA (inset of Fig. 17b) by subjecting to 1000 cycles. A stable GCD curves were attained upto 1000 cycles. % of Capacity retention at 1000th cycle was found to be 92%, shown in Fig. 17b.

In supercapacitors and batteries, a Ragone diagram, a plot of power density and energy density, was plotted. It facilitates the assessment of electrochemical energy storage performance of various energy storage devices. Here, a ragone diagram was plotted to recognize the variation of power density and energy density corresponding to the different C_s 's of LiZnVO_4 NPs-based supercapacitor obtained from several GCD's, shown in the inset of Fig. 17c. Power density and energy density at a C_s of 88.7 F/g were found to be 0.51 W/g and 12.3 Wh/Kg, respectively.

All these features recommend that of LiZnVO_4 NPs-based supercapacitor preserves the stability upto 1000 cycles of GCD's and is therefore well suited for electrochemical pseudocapacitive energy storage applications.

8 Humidity sensing of LiZnVO_4 NPs:

A cylindrical disc of LiZnVO_4 NPs was made using hydraulic press. It has nearly 8 mm of diameter and a 1.5 mm width. Ohmic connections on either faces of the disc were made by painting the silver paste and its humidity sensing parameters were measured using indigenous experimental setup, shown in Fig. 18. The arrangement showing glass chambers containing various saturated solutions to maintain specific % relative humidity (%RH) and are monitored by humidity meter (Mextech-DT-615). Every glass chamber was connected to a holding apparatus along with a rubber cork in order to hold the disc. The other ends of the electrodes are connected to a digital multimeter (Hioki DT 4282, Japan) to measure its electrical resistance before and after exposure of the sample to a specific %RH at ambient temperature.

LiZnVO_4 NPs was examined for the humidity sensing performance. Figure 19 shows a plot of resistance of LiZnVO_4 versus % RH conditions. A resistance of 28 M Ω was obtained at 11.0%RH and

this value found decreasing with the increase in %RH. At %RH of 97, resistance of LiZnVO_4 was found to be 1 M Ω , which is extremely low. This significant drop in resistance enhances the extent of conductivity of LiZnVO_4 because of the adsorption of water vapors on the sample surface due to the presence of open pores as revealed from its SEM image. The sensitivity factor (S_f) was calculated using the Eq. (6) and it was found to be 28. Using the method of the least square fit, the real sensitivity was calculated and found to be 0.3 M Ω /%RH. A correlation coefficient $R^2 = 0.997$ was obtained. Also, variation of resistance of the sample with %RH showing an excellent linearity suggests the significant sensitivity of the material. Limit of detection (LOD) of the sample was determined using the standard error estimation method [29] and was found to be 5%RH. Such good sensitivity, linearity and low LOD signify that LiZnVO_4 is well-structured material for fabrication of humidity sensors practicable at room temperature.

$$S_i = \frac{R_i}{R_f} \quad (6)$$

where, R_i is the initial resistance at 11%RH and R_f is the final resistance at 97%RH, respectively.

The falling in resistance of LiZnVO_4 with relative humidity is owing to the Grotthuss chain mechanism illustrated in Fig. 20. As relative humidity increases from 11 to 95% RH, resistance of LiZnVO_4 found decreased, which is a normal trend. This means the conductivity of the material increases, with an increase in RH at room temperature, is because of adsorption of H_2O molecules on the planes of LiZnVO_4 disc. Besides, these physisorbed water molecules undergoes ionization due to the strong electric field and high local charge density resulting in the production of hydronium ions (H_3O^+) in a greater extent and act as charge carriers by a sequence of exchange reactions. The presence of this type of protonic conduction in the adsorbed layers of water increases the conductivity and decreases the resistance drastically at higher RH [30].

Apart from sensitivity studies, studies on timing behavior of LiZnVO_4 are crucial for designing an effective humidity sensor Fig. 21. Depicts the typical response and recovery curves of the LiZnVO_4 at room temperature. The response and recovery times recorded for the LiZnVO_4 sample were 20 s and 27 s respectively. A rapid timing performance was due to

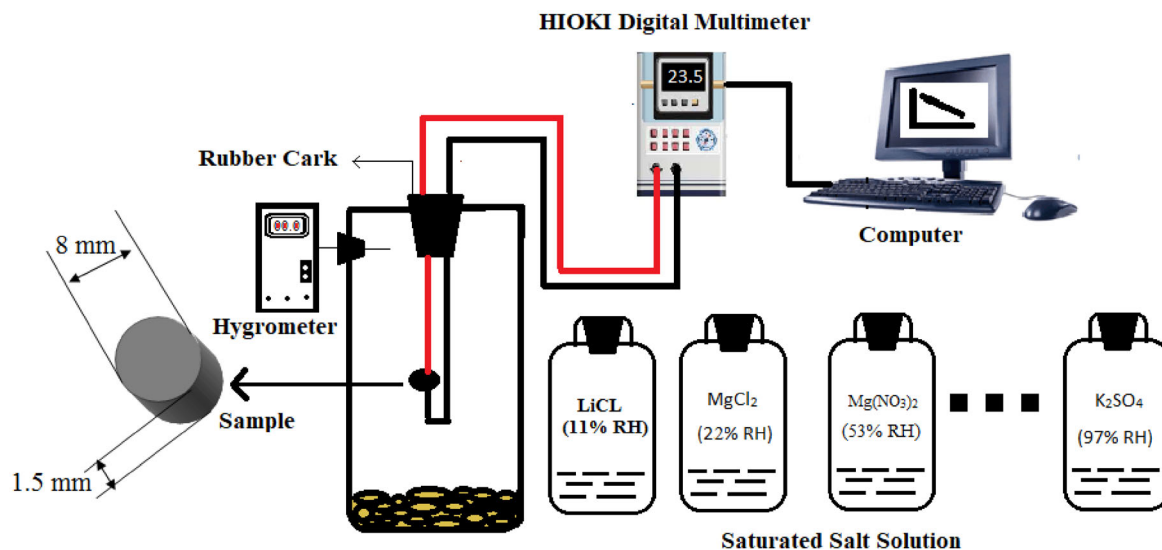


Fig. 18 Schematic representation of the humidity sensing measurement setup

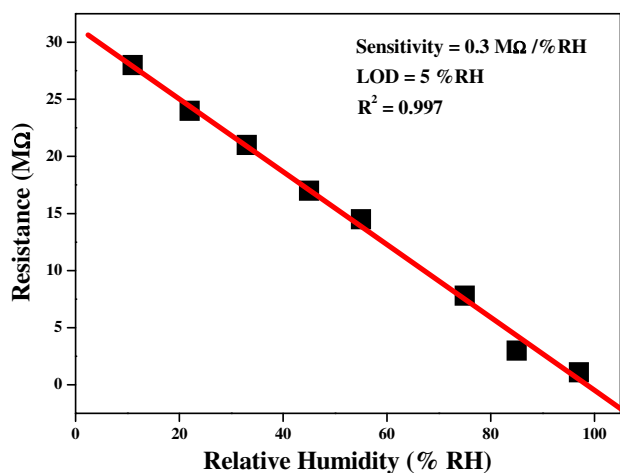


Fig. 19 Fall of resistance with increase in relative humidity

the presence of open pores on its surface for easy diffusion of water vapors, as discovered from its SEM studies. In addition, adsorption is spontaneous whereas desorption process takes an additional 7 s, as it requires extra energy to break the bonds formed between the surface of LiZnVO_4 and water molecules adsorbed on it [31].

Stability of LiZnVO_4 towards humidity sensing was examined by recording its resistance for every five days in all RH conditions, over a period of 1 month. From the Fig. 22, it was confirmed that LiZnVO_4 NPs show superior sensing stability. This effective, stable performance offers an additional advantage which further promotes the development of LiZnVO_4 based humidity sensors.

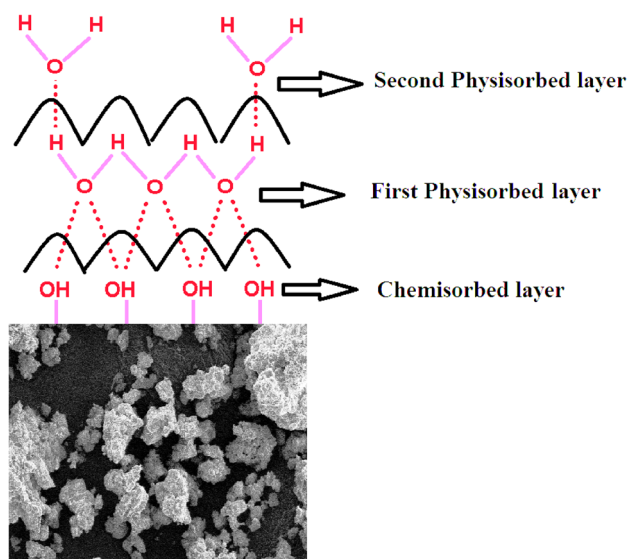


Fig. 20 Illustration showing Grotthuss chain mechanism in LiZnVO_4 NPs

9 Conclusion

We have successfully synthesized LiZnVO_4 NPs by employing the simple solution combustion method utilizing *Hibiscus* leaves as a combustible fuel. XRD assures the formation of the rhombohedral phenacite structure of the product. FT-IR strengthens the presence of the Zn–O and Li–VO₄ bonds. The produced LiZnVO_4 NPs exhibited significant antioxidant activity with the lowest IC_{50} , 37.32 $\mu\text{g}/\text{mL}$. It has the advantages of developing latent fingerprints for crime investigations. LiZnVO_4 NPs were used to

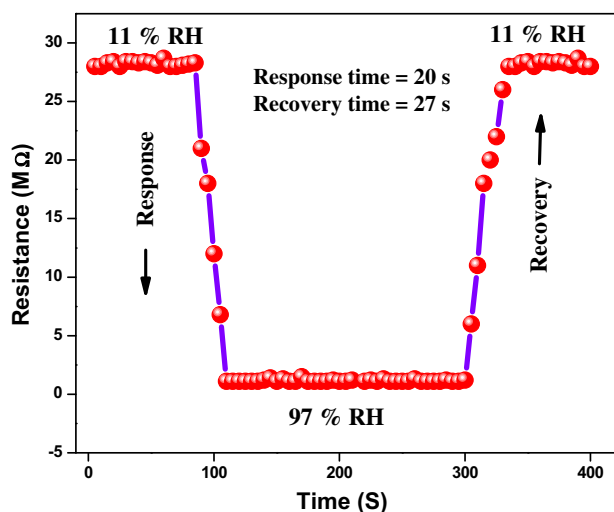


Fig. 21 Timing behavior of LiZnVO₄ NPs

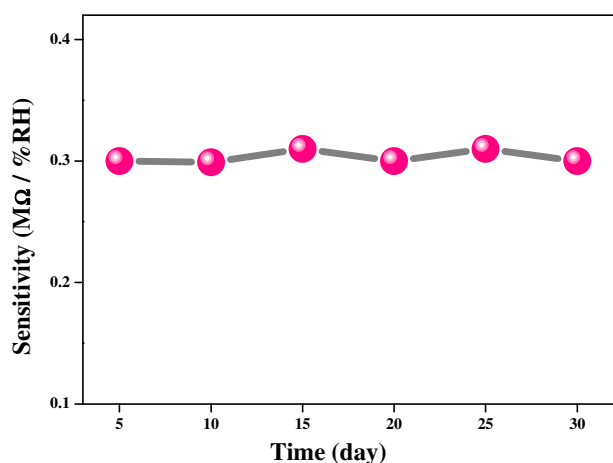


Fig. 22 Humidity sensing stability of LiZnVO₄ NPs

fabricate green emission LED. It is fruitful in examining the applicability of the LiZnVO₄ NPs based sensors in the electro analytic detection of nitrite at a lower concentration level. The specific capacitance and energy density of LiZnVO₄ electrode was found to be 11.034 F/g and 8.83 mWhkg⁻¹ at a scan rate of 20 mVs⁻¹ and 88.7 F/g at a current density of 0.1 mA. Power density and energy densities were found to be 0.51 W/g and 12.3 Wh/Kg, respectively. Hence, LiZnVO₄ NPs were also well suited for electrochemical pseudo-capacitive energy storage applications. Finally, it shows an excellent outcome of the humidity sensing of LiZnVO₄ with a very high sensitivity factor implies higher the sensitivity of the material towards the moisture, making it an outstanding candidate for the fabrication of current humidity sensors. Therefore, LiZnVO₄ NPs can be

used for multiple applications such as, optical, biological, electrochemical and energy storage applications.

Acknowledgements

Soundarya T L indebted to Principal, CEO and Director, Siddaganga Institute of Technology for extending laboratory and characterization facilities. G Nagaraju thanks to DST Nanomission, Govt. of India, New Delhi for financial support (No.SR/NM/NS-1262/2013). Authors also thank DST-SAIF, KOCHI and Center of Applied Research and nano-Technology, S.I.T, Tumakuru for TEM and SEM analysis.

Author Contribution

Material development, data collection, data analysis, writing were performed by TLS. Editing and reviewing by CU. Humidity sensing its analysis was performed by YTR. BN and GN Research administration.

Data availability

All data obtained during the analysis are in original format and can be accessed upon reasonable request from the corresponding author.

Declarations

Conflict of interest All authors affirm that they have no compete of interest.

References

1. Phaniendra, et al., Free radicals properties, sources, targets, and their implication in various diseases. *Ind. J. Clinic Biochem* **30**(1), 11–26 (2015)
2. X. Luo et al., Application of nanoparticles in electrochemical sensors and biosensors. *Electroanal. Int. J. Devoted Fund. Pract. Aspects Electroanal.* **18**(4), 319–326 (2006)
3. J.J. Sindelar et al., Human safety controversies surrounding nitrate and nitrite in the diet. *Nitric Oxide* **26**(4), 259–266 (2012)
4. P.S. Adarakatti et al., Amino-calixarene-modified graphitic carbon as a novel electrochemical interface for simultaneous

- measurement of lead and cadmium ions at picomolar level. *J Solid State Electrochem* **20**(12), 3349–3358 (2016)
- L. Zeng et al., Hierarchical LiZnVO₄@C nanostructures with enhanced cycling stability for lithium-ion batteries. *Dalton Trans.* **44**(17), 7967–7972 (2015)
 - Y. Lin et al., A new anode material LiZnVO₄: synthesis and electrochemical measurements. *Ionics* **19**(3), 391–394 (2013)
 - D. Guyomard, et al., *New amorphous oxides as high capacity negative electrodes for lithium batteries the Li_xMVO₄ (M= Ni, Co, Cd, Zn; 1 < x ≤ 8) series.* *Journal of power sources*, 1997 **68**(2): 692–697
 - S. Khurshid et al., Effect of Synthesis Methods on Structural, Optical and Spectral Properties of Bluish-Green LiZnVO₄ Phosphor. *Materials Focus* **5**(5), 485–488 (2016)
 - G. Viacava et al., Antioxidant activity of butterhead lettuce: evaluation of significant factors affecting antioxidant extraction and quantification. *J Food Meas Characterization* **9**(2), 206–214 (2015)
 - S. Kundu et al., A planar supercapacitor made of supramolecular nanofibre based solid electrolyte exhibiting 8 V window. *Nano Energy* **61**, 259–266 (2019)
 - U. Holzwarth et al., The Scherrer equation versus the 'Debye-Scherrer equation'. *Nat Nanotechnol* **6**(9), 534–534 (2011)
 - K.S. Babu et al., Synthesis and optical characterization of porous ZnO. *J. Adv. Ceram.* **2**(3), 260–265 (2013)
 - B. Grandhe et al., Spectral characterization of novel LiZnVO₄ phosphor. *Optics Communications* **285**(6), 1194–1198 (2012)
 - C.B. Rodella et al., V₂O₅/TiO₂ catalytic xerogels Raman and EPR studies. *J. sol-gel Sci. Technol.* **25**(1), 83–88 (2002)
 - R. Zamiri et al., Far-infrared optical constants of ZnO and ZnO/Ag nanostructures. *RSC Adv.* **4**(40), 20902–20908 (2014)
 - H. Sasabe et al., High power efficiency blue-to-green organic light-emitting diodes using isonicotinonitrile-based fluorescent emitters. *Chem. An Asian J.* **12**(6), 648–654 (2017)
 - H.J. Bolink et al., Green light-emitting solid-state electrochemical cell obtained from a homoleptic iridium (III) complex containing ionically charged ligands. *Chem Mater* **18**(12), 2778–2780 (2006)
 - K. Jongseong et al., Phenothiazine derivatives as an easily accessible emitter for green light-emitting electrochemical cells. *J. Luminescence* **197**, 383–388 (2018)
 - H.S. Yogananda et al., New design of highly sensitive and selective MoO₃: Eu³⁺ micro-rods: Probing of latent fingerprints visualization and anti-counterfeiting applications. *J. Colloid Inter. Sci.* **528**, 443–456 (2018)
 - E. Prabakaran et al., Nanomaterials for latent fingerprint detection: a review. *J. Mater. Res. Technol.* **12**, 1856–1885 (2021)
 - P. Sharma et al., DPPH antioxidant assay revisited. *Food Chem.* **113**(4), 1202–1205 (2009)
 - P. Ionita et al., Is DPPH stable free radical a good scavenger for oxygen active species. *Chem Pap* **59**(1), 11–16 (2005)
 - M. Zamani et al., Scavenging performance and antioxidant activity of γ -alumina nanoparticles towards DPPH free radical: Spectroscopic and DFT-D studies. *Spectrochimica Acta Part A* **201**, 288–299 (2018)
 - O.E. Adebisi et al., In vitro antioxidant activity, total phenolic and flavonoid contents of ethanol extract of stem and leaf of *Grewia carpinifolia* Beni-Suef University. *J. Basic Appl. Sci.* **6**(1), 10–14 (2017)
 - A. Matuszewska et al., Anticancer, antioxidant, and antibacterial activities of low molecular weight bioactive subfractions isolated from cultures of wood degrading fungus *Cerrena unicolor*. *PLoS ONE* **13**(6), e0197044 (2018)
 - C. Wei et al., Simultaneous electrochemical determination of hydroquinone, catechol and resorcinol at Nafion/multi-walled carbon nanotubes/carbon dots/multi-walled carbon nanotubes modified glassy carbon electrode. *Electrochim. Acta* **149**, 237–244 (2014)
 - A.A. Rafati et al., Simultaneous determination of ascorbic acid, dopamine, and uric acid using a carbon paste electrode modified with multiwalled carbon nanotubes, ionic liquid, and palladium nanoparticles. *Microchim. Acta* **181**(15–16), 1999–2008 (2014)
 - T.M. Dinh et al., High-resolution on-chip supercapacitors with ultra-high scan rate ability. *J. Mater. Chem. A* **2**(20), 7170–7174 (2014)
 - B. Chethan et al., Humidity sensing performance of hybrid nanorods of polyaniline-Yttrium oxide composite prepared by mechanical mixing method. *Talanta* **215**, 120906 (2020)
 - T. Divya et al., Nanoceria based thin films as efficient humidity sensors. *Sens. Actuat A: Phys* **261**, 85–93 (2017)
 - Chethan, et al., Polypyrrole based core-shell structured composite based humidity Sensor operable at room temperature. *Sens. Actuators B* **296**, 1266 (2019)

Publisher's Note Springer Nature remains neutral with regard to jurisdictional claims in published maps and institutional affiliations.